Quantum mechanical and crossed beam study of vibrational excitation of N_2 by electron impact at 30–75 eV*

Donald G. Truhlar† and Maynard A. Brandt

Department of Chemistry, University of Minnesota, Minneapolis, Minnesota 55455

Santosh K. Srivastava, S. Trajmar, and A. Chutjian

Jet Propulsion Laboratory, California Institute of Technology, Pasadena, California 91103
(Received 12 May 1976)

The ratios of differential cross sections for excitation of the first excited vibrational state and for elastic scattering for electron impact on N_2 have been measured at scattering angles ranging from 20° to 135° at 30, 35, 40, 45, and 75 eV impact energies and from 25° to 90° scattering angle at 20 eV impact energy. The results at 20 eV are in good agreement with two previous sets of measurements. Using previously measured and normalized elastic differential cross sections for N_2, the ratios have been converted to inelastic cross sections. Calculations using a four-state vibrational–rotational basis set and an effective interaction potential developed previously are reported at the five energies in the 30–75 eV region. It is shown that the potential scattering model can account for the magnitude and the qualitative behavior of the cross sections at 35–75 eV but there are some significant quantitative differences between theory and experiment. The most striking of these is the way the theoretical model overestimates the scattering at scattering angles less than about 50°. Core-excited resonances apparently make an appreciable contribution to the vibrationally inelastic scattering at 30 eV.

I. INTRODUCTION

The intermediate impact energy region (15 eV $\lesssim E_0 \lesssim$ 100 eV, where E_0 is the impact energy) is an important one for electron impact spectroscopy[1–3] as a tool for studying electronic excitation of molecules. Vibrational excitation of the ground electronic state has received little attention in this energy region but it can provide a good test of quantum mechanical descriptions of the scattering process and is used for such a test in the present article.

Previous work[4–5] on vibrational excitation of molecules at intermediate impact energies has been concerned with H_2 (experiment[2,4] and theory[2,4,5]), N_2 (experiment[2,6,10,11] and theory[10–12]), O_2 (experiment[6,9]), CO (experiment[6,11,13] and theory[11,13]), NO (experiment[6]), H_2O (experiment[7,14] and theory[15]), and CO_2 (experiment[7]). The present article reports new experimental and theoretical work for N_2, primarily in the impact energy region 30–75 eV and with additional new measurements at 20 eV. At lower energies the vibrational excitation of N_2 is dominated by various resonance processes[16] but there are a few "windows" between these resonance regions. A study of the nonresonant vibrational excitation in two of these windows (5 and 10 eV) is presented elsewhere.[17] In the present article we test how well the vibrational excitation at $E_0 \geq 30$ eV can be explained using a nonresonant model which has previously[18] been applied to the elastic scattering and rotational excitation.

II. EXPERIMENTAL PROCEDURE AND RESULTS

The electron-impact spectrometer used in the present study employs a crossed electron–molecule beam type of scattering geometry. The spectrometer, details of the electron optics, and the method of data acquisition have been described earlier.[19,20] Briefly, an electron beam of desired energy E_0 and spread ΔE_0 is focused onto the target N_2 beam, and the electrons scattered into a small solid angle ($\lesssim 10^{-3}$ sr) at an angle θ are energy-analyzed and detected by a spiraltron electron multiplier. The resulting pulses are amplified, counted, and recorded by a multichannel scaler as a function of energy loss. Each energy-loss spectrum is the result of many repetitive scans. The N_2 beam source was a multichannel array at room temperature and had a 3 torr back pressure. Thus the beam is cooled slightly by expansion. For the spectra reported here, E_0 was fixed at 30 eV, 35 eV, 45 eV, 50 eV, and 75 eV where θ was varied from 20° to 135° and at 20 eV where θ was fixed at 25°, 50°, and 90°. The overall resolution of the spectrometer was between 50 meV and 60 meV (FWHM). This is insufficient to resolve rotational excitations (or deexcitations) so the measurements are interpreted in terms of "vibrationally elastic" and "vibrationally inelastic" features. The former is the sum of pure elastic scattering and pure rotational excitation and deexcitation while the latter is the sum of pure vibrational excitation and vibrational–rotational excitation for a given final vibrational quantum number v'.

Two typical spectra for 30 eV impact energy and 20° and 90° scattering angles are shown in Fig. 1. Both elastically scattered electrons and the electrons responsible for the $v' = 1$ excitations are shown. It is clear from this figure that the intensity of the vibrational feature is quite weak in comparison with the elastic feature and there is some contribution to the former from the tail of the latter. The contribution to the vibrational intensity by the elastic scattering was estimated by drawing a smooth curve in the fashion shown by the dotted line in Fig. 1. The profile of the vibrational feature was considerably influenced by noise.

The ratio of the intensity corresponding to the $v' = 1$

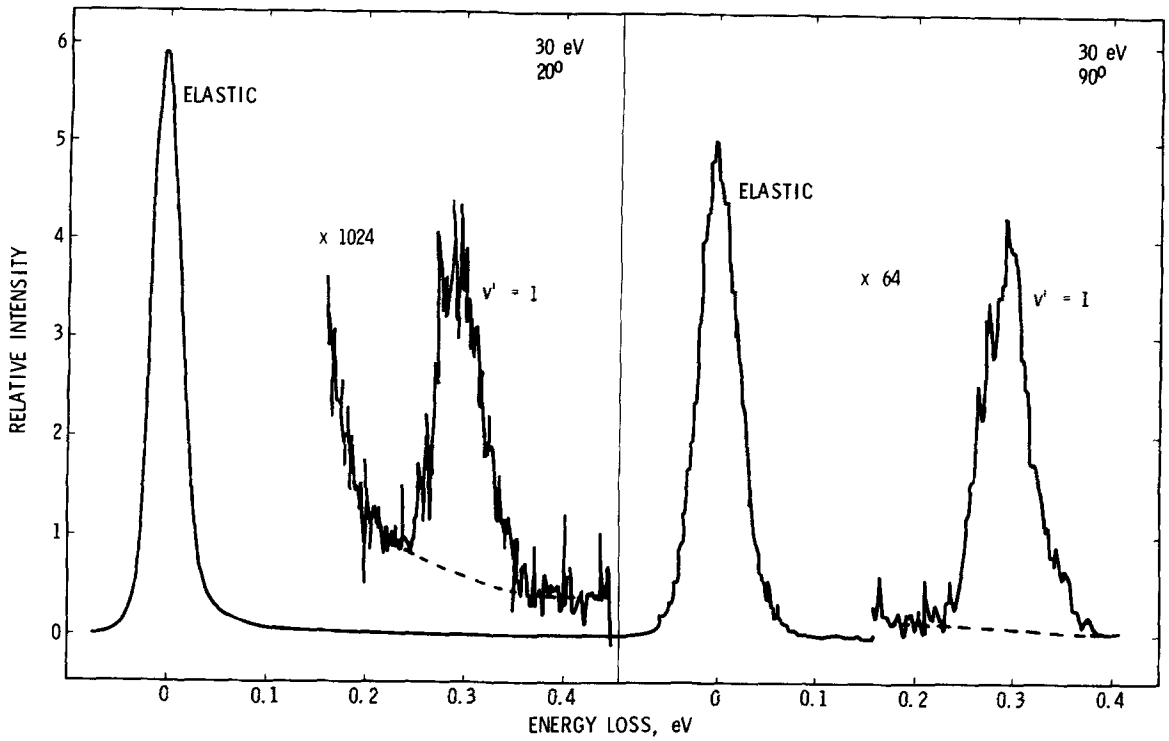

FIG. 1. Energy-loss spectrum of N_2 at an impact energy of 30 eV and scattering angles of 20° and 90°. The feature corresponding to vibrationally inelastic scattering to the first excited vibrational state is labeled $v' = 1$.

excitation to that corresponding to elastic scattering was measured by drawing a visually smooth profile of the vibrational-excitation feature and measuring its peak height and the peak height of the elastic feature. Full widths at half maxima for the elastic and $v' = 1$ features were also checked. Further, as discussed in the next paragraph, although the scattered intensity corresponding to vibrational excitation is typically only 10^{-3} times as large as that corresponding to elastic scattering, it was verified that the efficiency of the counting system does not depend on the rate at which the pulses arrive at the detector. Thus the ratio $R_1(E_0, \theta)$ of the respective differential cross sections defined by

$$R_1(E_0, \theta) \equiv \frac{d\sigma_{01}}{d\Omega}(E_0, \theta)\left(\frac{d\sigma_{00}}{d\Omega}(E_0, \theta)\right)^{-1}$$

was set equal to the ratio of the peak heights, or when the peak widths were different, to the ratio of peak heights times the ratio of peak widths. The absolute value of the cross section for excitation to the $v' = 1$ state was then obtained by multiplying the ratio by the absolute value of the elastic scattering cross section reported earlier.[21] The results are presented in Tables I and II.

The following precautions were taken to reduce the possible sources of errors in the measurements: (1) The energy of the incident electron beam was calibrated using the 19.35 eV resonance in helium. (2) The true zero scattering angle was determined from the symmetry of the scattering intensity corresponding to the $2\,^1P$ excitation in He. (3) The incident electron current was monitored by a Farady cup. It was found that the current was constant to within ±3% during the course of an experiment. (4) The contribution of the background scattering (both direct beam contribution and scattering by the background gas) was measured by providing an alternate leak to the vacuum chamber. The flow to the chamber was switched from the capillary array to the alternate gas inlet and the proper background pressure was established. At a fixed impact energy E_0, the angular distribution of elastically scattered electrons was measured. It was found that above 20° scattering angle the background scattering was negligible in comparison with the scattering from the beam formed by the capillary array. (5) In order to ensure that the efficiency of the detector system did not depend on the counting rate, we employed the following procedures. A pulse generator which could produce 100 nsec wide pulses with a wide range of repetition rates was connected to the input of the counting system (preamplifier, amplifier, discriminator, multichannel scalar). The number of pulses generated per second by the pulse generator was measured by an oscilloscope and at the same time counted through the multichannel scaling system over preset time intervals. The rate of pulse generation was then varied over three orders of magnitude. The pulse frequency values obtained by the two methods agreed to within the precision of the oscilloscope measurement. This test established that the efficiency of the pulse counting system was independent of pulse frequency. In order to establish the same property for the electron multiplier, the scattering intensity ratio of the inelastic to elastic features was determined at elastic-scattering count rates varying from 0.25 to 11.8 kHz, a range which included all count rates encountered in the present investigation. No dependence of the ratio on count rates was observed.

The following were the sources of error: (A) As

TABLE I. Ratio $R_1(E_0, \theta)$ of the differential cross section for vibrationally inelastic scattering to that for vibrationally elastic scattering as a function of impact energy E_0 and scattering angle θ.

θ(deg) \ E_0(eV)	30	35	45	50	75
20	5.4±0.6(−4)[a,b] 1.2(−3)[c]	2.0±0.2(−4) 1.4(−3)	1.4±0.2(−4) 1.0(−3)	1.6±0.2(−4) 7.7(−4)	3.2±0.4(−4) 3.8(−4)
30	8.1±1.1(−4) 9.8(−4)	2.0±0.2(−4) 1.3(−3)	3.0±0.4(−4) 1.3(−3)	2.7±0.5(−4) 1.0(−3)	5.9±0.6(−4) 5.6(−4)
40	1.4±0.2(−3) 8.9(−4)	n.a.[d] 1.3(−3)	n.a. 1.7(−3)	8.4±1.2(−4) 1.6(−3)	1.9±0.2(−3) 1.5(−3)
50	2.5±0.4(−3) 1.8(−3)	1.1±0.1(−3) 2.0(−3)	1.6±0.2(−3) 2.7(−3)	1.8±0.3(−3) 2.7(−3)	3.5±0.4(−3) 2.8(−3)
60	4.6±0.6(−3) 2.7(−3)	n.a. 2.9(−3)	n.a. 3.6(−3)	3.6±0.4(−3) 3.8(−3)	4.6±0.5(−3) 3.9(−3)
70	8.0±1.2(−3) 3.2(−3)	4.6±0.5(−3) 3.2(−3)	4.8±0.5(−3) 4.2(−3)	6.0±0.8(−3) 4.6(−3)	5.3±0.5(−3) 4.3(−3)
80	1.2±0.1(−2) 3.7(−3)	n.a. 3.6(−3)	n.a. 3.8(−3)	8.0±0.8(−3) 4.0(−3)	5.7±0.6(−3) 2.9(−3)
90	1.3±0.1(−2) 5.0(−3)	7.4±0.8(−3) 4.7(−3)	8.8±0.9(−3) 2.5(−3)	8.2±0.9(−3) 2.1(−3)	5.3±0.5(−3) 1.5(−3)
100	1.1±0.1(−2) 7.1(−3)	n.a. 6.5(−3)	n.a. 2.8(−3)	6.4±0.7(−3) 1.6(−3)	3.9±0.4(−3) 1.7(−3)
115	8.3±0.9(−3) 8.4(−3)	4.1±0.4(−3) 8.8(−3)	4.3±0.5(−3) 4.9(−3)	3.6±0.5(−3) 3.7(−3)	2.6±0.3(−3) 6.6(−3)
135	4.8±0.5(−3) 4.6(−3)	3.6±0.4(−3) 6.0(−3)	2.6±0.3(−3) 7.3(−3)	2.8±0.3(−3) 7.7(−3)	3.3±0.3(−3) 1.6(−2)

[a]Numbers in parentheses are multiplicative powers of 10.
[b]Upper entry is experimental result.
[c]Lower entry is theoretical result.
[d]n.a. denotes not available.

mentioned earlier, the noise contributed to the error in the ratio $R_1(E_0, \theta)$ of the two cross sections. This varied for each measurement. (B) An uncertainty was contributed by the presence of the tail of the elastic feature. (C) There was an uncertainty of ±1° in the measurement of the scattering angles. The error due to this also varied for each measurement. (D) The absolute values of elastic scattering cross sections were known with an estimated accuracy of ±15%. Since the value of $d\sigma_{01}/d\Omega(E_0, \theta)$ is obtained by multiplying the ratio $R_1(E_0, \theta)$ by the absolute value of $d\sigma_{00}/d\Omega(E_0, \theta)$ this uncertainty contributed to the error. The reader should recall that the vibrationally elastic cross sections[21] were normalized at each impact energy and scattering angle to the elastic scattering cross sections for He of McConkey and Preston.[22] Thus, should more accurate elastic scattering cross sections for He become available the present cross sections should be adjusted at each impact energy and scattering angle by the ratio of the more accurate cross section to that of McConkey and Preston. The overall error in $d\sigma_{01}/d\Omega(E_0, \theta)$ was calculated for each scattering angle θ and impact energy E_0 by taking the square root of the sum of the squares of each error. These are given in Table II.

III. THEORETICAL CALCULATIONS

A. Review of the model

The model and the methods used for the scattering calculations are described elsewhere.[18] Basically the calculations consist of applying the vibrational–rotational close-coupling method in the laboratory frame using a total-angular-momentum representation with unconverged state expansions and with an effective interaction potential. The vibrational–rotational close-coupling method in the laboratory frame using a total-angular-momentum representation consists of expanding the total system wavefunction as a sum of products of radial translational functions times channel functions (functions of the angular, rotational, and vibrational coordinates times a ground-electronic-state electronic wavefunction) which are eigenfunctions of total orbital angular momentum (with associated quantum number J). Contributions from $J=0$ to $J=J_{max}$ are included. Our calculations are converged with respect to increasing J_{max}. If our effective interaction potential were the correct generalized optical potential our calculations would be exact. The correct generalized optical potential may be considered to consist of five parts: (i) the static or first-order potential, (ii) an exchange potential to account for exchange of the incident electron with bound ones, (iii) the real polarization potential which accounts for virtual charge-cloud polarization of the target, (iv) the imaginary polarization potential which accounts for real excitation of excited electronic states, (v) a contribution to account for the effect of those excited vibrational–rotational states not explicitly included in the state expansion. In the exact potential, parts (ii)–(v) are nonlocal. Parts

TABLE II. Experimental and theoretical differential scattering cross sections for $0 \rightarrow 1$ vibrational excitation of N_2 as functions of impact energy E_0 and scattering angle θ.

θ(deg) \ E_0(eV)	$[d\sigma_{01}/d\Omega](E_0,\theta)(10^{-3}a_0^2/\mathrm{sr})$ 30	35	45	50	75
	Angles at which experiment and theory are available				
20	6.9 ± 1.3[a]	2.5 ± 0.5	1.7 ± 0.3	1.9 ± 0.3	3.2 ± 0.6
	17.5[b]	22.1	17.5	13.8	6.92
30	5.8 ± 1.2	1.3 ± 0.2	1.8 ± 0.4	1.5 ± 0.4	2.2 ± 0.5
	6.56	9.45	9.64	7.90	3.91
40	5.4 ± 1.5	n.a.[c]	n.a.	2.2 ± 0.5	3.0 ± 0.6
	3.12	4.46	6.07	5.84	5.00
50	5.4 ± 1.2	1.9 ± 0.4	2.2 ± 0.5	2.4 ± 0.6	2.5 ± 0.5
	4.55	5.18	6.87	6.96	6.67
60	5.9 ± 1.1	n.a.	n.a.	2.7 ± 0.5	2.1 ± 0.4
	6.15	6.84	8.32	8.69	7.28
70	6.0 ± 1.3	3.0 ± 0.5	2.4 ± 0.4	2.8 ± 0.5	1.5 ± 0.3
	6.07	6.47	8.11	8.45	6.21
80	6.6 ± 1.2	n.a.	n.a.	2.9 ± 0.5	1.6 ± 0.3
	5.61	5.38	5.52	5.51	3.38
90	5.9 ± 1.1	2.8 ± 0.5	2.4 ± 0.4	2.1 ± 0.4	1.7 ± 0.3
	6.73	5.98	3.12	2.45	1.42
100	5.3 ± 1.0	n.a.	n.a.	2.1 ± 0.4	1.1 ± 0.2
	9.61	8.95	3.66	1.97	1.34
115	7.7 ± 1.4	3.2 ± 0.6	3.1 ± 0.6	3.0 ± 0.6	1.5 ± 0.3
	12.6	13.1	7.21	4.96	3.47
135	11.5 ± 2.1	8.2 ± 1.5	5.9 ± 1.1	6.5 ± 1.2	5.1 ± 0.9
	5.94	6.72	6.05	5.32	3.55
	Angles at which only theory is available				
0	48.2	47.5	32.7	28.1	30.2
15	25.4	30.6	22.3	17.4	11.7
150	1.64	3.35	7.48	7.73	3.49
180	8.61	16.1	27.8	27.5	12.4

[a]Upper entry is experimental result.
[b]Lower entry is theoretical result.
[c]n. a. denotes not available.

(iii)–(v) are difficult to obtain and obtaining them exactly would be essentially equivalent to solving the scattering problem excatly. The present model does not explicitly include parts (ii), (iv), and (v). We use a reasonably accurate static potential calculated as a function of N_2 internuclear separation by the INDO/1*s* method[18,23] (which includes exchange of bound electrons among themselves). For the real polarization potential we use the local model potential of Burke and Chandra.[24] This is proportional to the molecular static electric dipole polarizability and contains a parameter they adjusted in fixed-nuclei calculations to the Π_g resonance at 2.4 eV. Their polarization potential is not as strong at small distances as the complete adiabatic one would be there. Our justification for using at 30–75 eV a nonadiabatic polarization potential adjusted at 2.4 eV is that, to a first approximation at low and intermediate energies, the nonadiabatic correction to the adiabatic polarization potential is independent of impact energy. This is discussed elsewhere.[25] In the calculations of Burke and Chandra the N_2 was treated as a rigid rotator (such a calculation is inapplicable to vibrational excitation). For the present calculations we require the polarization potential as a function of N_2 internuclear separation so it was assumed[18] that this functional dependence is due entirely to the dependence of the molecular static electric dipole polarizability on internuclear separation. Additional details are given elsewhere.[18]

We can summarize our approximations as (a) neglect of exchange, (b) approximation of the nonlocal complex polarization potential by a real local model potential, and (c) nonconvergence of the vibrational–rotational state expansion. Approximation (a) is expected to become less serious as the energy increases. Its effect could be most easily assessed by using approximations[26] to the exchange potential which are energy dependent but local in the coordinate representation. The present calculations may actually include (in a crude way) some of the effect of exchange because Burke and Chandra neglected exchange in their treatment of the Π_g scattering and therefore their semiempirical polarization potential is really adjusted to account for both polarization and exchange. Since the effect of exchange is smaller at intermediate energy than at low energy,[26] this is not an accurate way to include exchange. Approximation (b) is the most difficult to assess theoretically and the comparison of the present calculations to experiment is one attempt to assess it. Part (v) of the correct generalized optical potential would vanish and thus approximation (c) would vanish if the size of the vibrational–rotational basis used in the close-coupling calculations were increased to convergence. This was not done because we wanted to test a model for which computer-time costs are not too large and which is practical even for more complicated molecules. In order to learn more about this source of error it is necessary to compute cross sections for various sizes of the vibrational–rotational basis.

B. Calculations and results

As in our treatment[18] of pure elastic scattering and rotational excitation, in the present calculations we truncated the close-coupling equations with four states corresponding to (v, j) of (0, 0), (0, 2), (1, 0), and (1, 2). This is called the 4VR basis set. In practice the vibrational–rotational state expansion is slowly convergent only at low J.[18] In particular we found that for $J > J_1$ (where J_1 increases slowly with energy and is in the range 8–11) the contribution to vibrational–rotational excitation is negligible (less than about 1%) and the contribution to pure vibrational excitation [(0, 0) → (1, 0)] is adequately approximated using only two states in the state expansion. This is called the 2 V basis. We consider the ground vibrational–rotational state to be the initial state (see the Appendix for a test of this assumption) and we calculate the vibrationally inelastic differential cross section $d\sigma_{01}/d\Omega(E_0, \theta)$ as the sum of the pure vibrational excitation and the vibrational–rotational excitation. At 30 and 50 eV we calculate the $d\sigma_{01}/d\Omega(E_0, \theta)$ using the 4 VR basis for $0 \leq J \leq J_1$ and the 2 V basis for $(J_1 + 1) \leq J \leq 20$. The contribution of the latter range of J values to the differential cross section was found to be relatively small (less than about 5%). At the other energies we included only $J \leq J_1$ in the calculations.

We computed vibrationally inelastic integral cross sections $\sigma_{0v'}(E_0)$ and vibrationally inelastic contributions

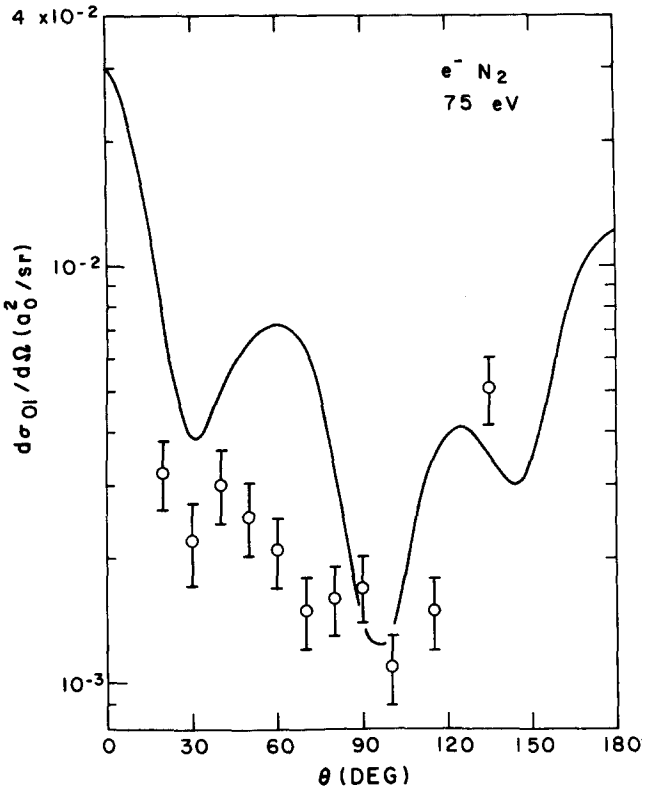

FIG. 2. Differential cross section for vibrationally inelastic scattering at $E_0 = 75$ eV as a function of scattering angle. Solid line is the theoretical result calculated at the 4VR level of approximation. Circles are the experimental results. The error estimates for the experimental data are given in Table II.

$\sigma^m_{0v'}(E_0)$ to the momentum transfer cross sections using the definitions

$$\sigma_{0v'}(E_0) = 2\pi \int_{0°}^{180°} \frac{d\sigma_{0v'}}{d\Omega}(E_0,\ \theta) \sin\theta\, d\theta\ , \tag{1}$$

$$\sigma^m_{0v'}(E_0) = 2\pi \int_{0°}^{180°} \frac{d\sigma_{0v'}}{d\Omega}(E_0,\ \theta)(1-\cos\theta) \sin\theta\, d\theta\ , \tag{2}$$

In Eq. (2) we made the common approximation of replacing $[1-(k'/k)\cos\theta]$, where k'/k is the ratio of final and initial momenta, by $(1-\cos\theta)$, which makes negligible difference. The integral and momentum-transfer cross sections converge more rapidly than the differential cross sections; e.g., we found that converged integral cross sections at 30 and 50 eV can be obtained including only $0 \le J \le 5$.

The differential cross sections are given in Table II and Fig. 2, their ratio to the vibrationally elastic differential cross sections[18] is given in Table I, and the integral and momentum transfer cross sections are given in Table III. The vibrationally inelastic cross sections are dominated in the forward direction by pure vibrational excitation. The differential cross sections for vibrational–rotational excitation are not so forward peaked but make appreciable contributions to vibrationally inelastic scattering at other angles; they range from $0.4\times10^{-3}\ a_0^2$/sr at 75 eV, 80° and 50 eV, 100° to $6.6\times10^{-3}\ a_0^2$/sr at 45 eV, 180°. At all five energies, vibrational–rotational excitation contributes 47–50% of the vibrationally inelastic integral cross section.

C. Experimental integral cross sections

Since the experimental differential cross sections $d\sigma_{01}^{exp}/d\Omega(E_0,\ \theta)$ are not available over the whole angular range, some extrapolation is necessary to obtain experimental integral cross sections. At small angles this was accomplished using differential cross sections $\sigma_{01}^{4VR}(E_0,\ \theta)$ obtained from the 4VR calculations as follows:

$$\frac{d\sigma_{01}^{exp}}{d\Omega}(E_0,\ \theta) = \frac{d\sigma_{01}^{4VR}}{d\Omega}(E_0,\ \theta) \times \left[\frac{d\sigma_{01}^{exp}}{d\Omega(E_0,\ 20°)}\right]\left[\frac{d\sigma_{01}^{4VR}}{d\Omega(E_0,\ 20°)}\right]^{-1},\quad \theta < 20°$$

At large angles two different methods were used:

$$\frac{d\sigma_{01}^{exp}}{d\Omega}(E_0,\ \theta) = \frac{d\sigma_{01}^{4VR}}{d\Omega}(E_0,\ \theta)\,\frac{d\sigma_{01}^{exp}}{d\Omega}(E_0,\ 135°) \times \left[\frac{d\sigma_{01}^{4VR}}{d\Omega}(E_0,\ 135°)\right]^{-1},\quad \theta > 135° \text{ (method I).}$$

$$\frac{d\sigma_{01}^{exp}}{d\Omega}(E_0,\ \theta) = \frac{d\sigma_{01}^{exp}}{d\Omega}(E_0,\ 135°),\quad \theta > 135° \text{ (method II).}$$

One reason for considering method II is that the experimental cross section increases when θ is increased from 115° to 135° but the 4VR one is decreasing at 135°. However, at even larger θ the 4VR differential cross section does increase. The experimental integral cross sections so obtained are given in Table III. The results obtained by method II range from 1.11–0.81 times those obtained by method I. There is insufficient experimental data at large θ to calculate an experimental value for the contribution of vibrational excitation to the momentum transfer cross section.

IV. DISCUSSION

A. Comparison of present experimental results to previous ones

The only previous experimental results for vibrational excitation of N_2 in this energy range are those of Skerbele, Dillon, and Lassettre[6] for R_1 (45 eV, θ) for θ equals 3–14° and those of Pavlović *et al.*[10] for $R_{v'}(E_0,\ \theta)$ and $d\sigma_{0v'}/d\Omega(E_0,\ \theta)$ at $E_0 \le 35$ eV and θ equals 25°, 50°, and 90°. The present experiments do not extend

TABLE III. $0 \rightarrow 1$ vibrational excitation of N_2: integral cross sections σ_{01} and contributions σ_{01}^m to momentum transfer cross sections.

	E_0(eV)				
	30	35	45	50	75
	$\sigma_{01}(10^{-2}\ a_0^2)$				
Theory (4VR[a])	9.7	10.8	9.5	8.4	5.7
Experiment (I[b])	8.4	4.5	4.6	5.1	3.6
Experiment (II[b])	9.4	4.7	4.0	4.1	3.3
Experiment (ave[b])	8.9	4.6	4.3	4.6	3.4
	$\sigma_{01}^m(10^{-2}\ a_0^2)$				
Theory (4VR[a])	9.2	10.2	9.1	8.0	4.9

[a] 4VR denotes the basis set (see Sec. III.B).
[b] I and II denote the method used for extrapolation in 135°–180° angular region (see Sec. II.C); ave denotes the average of the average of the two values.

TABLE IV. Comparison of ratios $R_1(E_0, \theta)$ of vibrationally inelastic to vibrationally elastic differential cross sections as functions of impact energy E_0 and scattering angle θ.

θ(deg) \ E_0(eV)		$10^4 R_1(E_0, \theta)$ 20	30	35	45	50	75
25	exp[a]	46	6.2	1.9	2.0	2.0	3.9
	PBHS[b]	40	7.9	1.2	n.a.	n.a.	n.a.
	4VR[c]	n.a.[d]	11	14	11	8.8	4.1
50	exp	81	25	11	16	18	32
	PBHS	85	17	1.3	n.a.	n.a.	n.a.
	4VR	n.a.	18	20	27	27	28
90	exp	268	128	74	88	82	57
	PBHS	210	66	1.0	n.a.	n.a.	n.a.
	4VR	n.a.	50	47	25	21	15

[a]Present experimental result.
[b]Experimental result of Pavlović, Boness, Herzenberg, and Schulz (Ref. 10).
[c]Present theoretical result.
[d]Not available.

to small enough angles to be directly compared to the experiments of Skerbele, Dillon, and Lassettre. They found R_1 (45 eV, θ) essentially independent of θ for small θ and equal to 4.3×10^{-4}. The present experimental results are $R_1(45\text{ eV}, 20°) = 1.4\times10^{-4}$ and $R_1(45\text{ eV}, 30°) = 3.0\times10^{-4}$ (see Table I). These results do not seem consistent. The source of discrepancy, if any, is unclear.

The present experimental results are compared to the results of Pavlović *et al.*[10] at 20, 30, and 35 eV in Tables IV (ratios) and V (cross sections). The agreement is best at 20 eV where the intensity associated with vibrational excitation is greatest. At this energy at 25° and 50° the agreement is very good but at 90° our vibrational excitation cross sections are appreciably larger than theirs. At 30 and 35 eV there is a large disagreement for the intensity ratios even though intensity ratios are generally considered to be the most reliably measurable quantities. We investigated various possible sources of errors (described in Sec. II) which could influence the values of these ratios, but it was found that these possible sources of error could not account for the disagreement. The vibrationally inelastic cross sections reported previously by two of us and Williams[11] at 20 eV are also listed in Table V. They are in good agreement with the present experimental results.

B. Comparison of experiment to theory

As shown by Table III the present theoretical integral cross sections are larger than experiment by about 10% at 30 eV and by about a factor of two at 35–75 eV. The experimental cross sections decrease by about a factor of two as the energy is increased from 30 eV to 35 eV, presumably[10–12,18] due to a core-excited resonance contribution at 30 eV and lower energies which is unimportant at energies of 35 eV and higher. The present theoretical treatment does not include resonances due to electronically excited cores so it is not surprising that the theoretical integral cross section does not show this sharp decrease in the 30–35 eV energy region. In fact since the present theoretical integral cross sections are too large in the nonresonant 35–75 eV region, the better agreement at 30 eV is apparently due at least in part to a cancellation of errors. Next we consider the 35–75 eV region which provides a better test of our theory for nonresonant excitation.

In the 35–75 eV region the theoretical and experimental integral cross sections agree within about a factor of 1.7–2.3. This is actually quite satisfactory considering that (i) these integral cross sections are only about 1.6×10^{-3} times the vibrationally elastic cross sections at the same energies and (ii) the theory contains no parameters adjusted in the intermediate energy region (the polarization potential does contain one parameter adjusted by Burke and Chandra[24] to the resonance at 2.4 eV).

The experimental differential cross sections provide a more stringent and more informative test of theory. Both the ratios and the absolute differential cross sections (Tables I and II) indicate that the theory fails most severely in the near-forward direction ($\theta \lesssim 50°$) where it appreciably overestimates the vibrational excitation cross section at 35–50 eV. For $\theta \geq 50°$ and $E_0 = 35$–75 eV, the theoretical value of the ratio $R_1(E_0, \theta)$ divided by the experimental one is in the range 0.36–4.0 in all cases for which comparison is possible; further this ratio is generally greater than 1.0 at θ equals 50°, 115°, and 135° and less than 1.0 at θ equals 60°–100°. For θ in the range 40° to 135° and E_0 in the range 35–75 eV the theory seems to always predict the correct order of magnitude of the differential cross section. Further the minimum in the calculated dif-

TABLE V. Comparison of differential scattering cross sections for $0 \rightarrow 1$ vibrational excitation of N_2 as functions of impact energy E_0 and scattering angle θ.

θ(deg) \ E_0(eV)		$[d\sigma_{01}/d\Omega](E_0, \theta)$ (10^{-3} a_0^2/sr) 20	30	35	45	50	75
25	exp[a]	44	5.9	1.8	1.7	1.7	2.4
	PBHS[b]	44	2.1	0.82	n.a.	n.a.	n.a.
	TTW[c]	48	n.a.	n.a.	n.a.	n.a.	n.a.
	4VR[d]	n.a.[e]	11	15	13	10	4.7
50	exp	26	5.4	1.9	2.2	2.4	2.5
	PBHS	23	1.3	0.22	n.a.	n.a.	n.a.
	TTW	28	n.a.	n.a.	n.a.	n.a.	n.a.
	4VR	n.a.	4.6	5.2	6.9	7.0	6.7
90	exp	19	5.9	2.8	2.4	2.1	1.7
	PBHS	11	1.3	0.09	n.a.	n.a.	n.a.
	TTW	22	n.a.	n.a.	n.a.	n.a.	n.a.
	4VR	n.a.	6.7	6.0	3.1	2.4	1.4

[a]Present experimental result.
[b]Experimental result of Pavlović, Boness, Herzenberg, and Schulz (Ref. 10).
[c]Experimental result reported by Truhlar, Trajmar, and Williams (Ref. 11); result at 90° is extrapolation from 80° using PBHS result for ratio of 90° cross section to 80° one.
[d]Present theoretical result.
[e]Not available.

TABLE VI. Differential cross section $d\sigma_{01}/d\Omega$ for the $0 \rightarrow 1$ vibrational excitation and its ratio R_1 to the vibrationally elastic differential cross section.[a]

		$10^4 R_1$					$[d\sigma_{01}/d\Omega](10^{-3}a_0^2/sr)$.				
		Experimental		Calculated			Experimental		Calculated		
E_0(eV)	θ(deg)	Previous	Present	b	c	Present	Previous	Present	b	c	Present
35	25	1.2(P)	1.9	8.6	8.5	14	0.82(P)	1.8	13	14	15
	50	1.3(P)	11	10.5	8.6	20	0.22(P)	1.9	1.5	3.3	5.2
	90	1.0(P)	74	68	8.2	47	0.09(P)	2.8	0.09	0.43	6.0
45	3	4.3(S)	...	8.4	8.4	5.9	...	...	57	50	32
	14	4.3(S)	...	8.5	8.5	8.5	...	...	25	24	23
	25	...	2.0	8.7	8.6	11	...	1.7	10.0	11	13
	50	...	15	13	8.5	27	...	2.2	0.71	2.2	6.9

[a]Previous experimental results are from: Pavlović, Boness, Herzenberg, and Schulz (Ref. 10), denoted P, and from Skerbele, Dillon and Lassettre (Ref. 6), denoted S. Previous calculated results are models b and c of Ref. 12.

ferential cross sections seem to be in about the right angular locations.

When we recall that this theoretical method did not predict the vibrationally elastic scattering[18] quantitatively accurately for $\theta > 50°$, the reasonably good agreement with experiment for the vibrationally inelastic scattering in this angular region is remarkable. A better treatment of vibrationally inelastic scattering would involve one theoretical model which simultaneously yields successful predictions for vibrationally elastic and inelastic scattering. Since the large-angle elastic scattering can apparently be treated accurately by treating well the scattering by the parts of the static potential near the nuclei,[27] we expect that the treatment of the large-angle scattering would be improved by including more calculated states in the wavefunction expansion in order to more accurately treat the asymmetry of the potential near the nuclei. Other indications of the necessity of including more rotational states are the large vibrational–rotational-excitation differential cross sections at large scattering angle and the large dependence of the vibrationally inelastic scattering on the initial rotational state (see Appendix).

The overestimation of the small-angle scattering is almost surely associated with some failure of the polarization potential. It is difficult to obtain a good polarization potential for elastic scattering. This difficulty is compounded for the present problem by the unknown dependence of the short-range part of the polarization potential on internuclear distance. Apparently a more fundamental approach to the problem of charge-cloud polarization will eventually be required.

We did not test the sensitivity of the results to the parameter in the polarization potential. It is, however, interesting that Crees and Moores[28] obtained results for the low-energy Π_g scattering in the absence of a polarization potential somewhat in disagreement with those of Burke and Chandra. If the calculations of Burke and Chandra are in error then our polarization potential is not adjusted to exactly reproduce the low-energy resonance. Nevertheless it is still a realistic polarization potential. However, it would be interesting to test the sensitivity of the present results to small variations of the polarization potential.

We have no quantitative estimate of the effect of electron exchange involving the scattering electron on the vibrational process considered here. Our previous (more approximate) work[4] on H_2 indicated the effect of exchange on σ_{01} was only about 10% in this energy region.

Finally we briefly compare to the only previous published calculations[12] of vibrational excitation of N_2 in this energy region. Those were plane-wave calculations employing considerably more simplified model potentials. The most justifiable of those model potentials are the ones due to Takayanagi and Geltman[29] (model b of Refs. 11 and 12) and Sampson and Mjolsness[30] (model c of Refs. 11 and 12). The present results are compared to the published plane-wave results employing those potentials in Table VI. This comparison shows that those simple calculations are about as accurate as the present ones except at large angles where the plane wave models are not expected[12] to be as accurate as at small angles. Nevertheless, the present calculations are more valuable because they are much closer to a completely justified theoretical treatment. Thus the two most important approximations of the previous work[11,12] are probably the oversimplified short-range potential and the use of plane-wave scattering states. But these approximations cannot be improved in either order. If one attempts to use an accurate short-range potential but still use plane-wave scattering states, the computed cross sections are much too large[31] because the plane-wave approximation is much less valid for a potential such as the present one which includes the strong interaction with the nuclei realistically than for the comparatively weak model potentials b and c. In contrast the present calculations are probably close enough to a complete treatment that the remaining approximations could reasonably be improved in any order.

V. CONCLUSION

We conclude that the $0 \rightarrow 1$ vibrational excitation of N_2 at 35–75 eV can be qualitatively explained using a potential scattering model involving a reasonable effective potential. However quantitative agreement of experiment and theory will apparently require a better

TABLE VII. Unaveraged and averaged calculations of vibrationally elastic and inelastic cross sections at 50 eV impact energy.

θ (deg)	$d\sigma_{00}/d\Omega$ (a_0^2/sr)	$d\sigma_{00}^{ave}/d\Omega$ (a_0^2/sr)	$d\sigma_{01}/d\Omega$ ($10^{-3}a_0^2$/sr)	$d\sigma_{01}^{ave}/d\Omega$ ($10^{-3}a_0^2$/sr)
5	50.5	52.5	25.6	22.3
10	37.0	29.8	21.2	19.6
20	17.9	20.9	13.8	14.0
30	7.63	9.86	7.90	9.18
40	3.54	4.68	5.84	6.56
50	2.54	2.90	6.96	7.14
60	2.25	2.27	8.69	9.78
70	1.84	1.81	8.45	11.0
80	1.39	1.32	5.51	8.74
90	1.19	1.02	2.45	5.34
100	1.26	1.02	1.97	4.13
110	1.36	1.15	3.83	5.97
120	1.24	1.18	5.75	7.91
130	0.88	0.96	5.76	7.72
140	0.56	0.68	5.16	7.16
150	0.62	0.64	7.73	10.9
	σ_{00} (a_0^2)	σ_{00}^{ave} (a_0^2)	σ_{01} ($10^{-3}a_0^2$)	σ_{01}^{ave} ($10^{-3}a_0^2$)
	36.7	39.8	84	111

treatment of polarization and inclusion of more than two rotational states in the expansion of the wavefunction. The experimental cross section for $0 \rightarrow 1$ vibrational excitation at 30 eV is about twice as great as that at 35 eV and this effect is not accounted for by our potential scattering model. This is consistent with the previous interpretation[10–12,16] that core-excited resonances make an appreciable contribution to the $0 \rightarrow 1$ vibrational excitation below about 33 eV.

ACKNOWLEDGMENTS

The authors are grateful to the late Professor George J. Schulz for supplying us with enlarged copies of the figures of Ref. 10 from which the values of $R_1(E_0, \theta)$ and $d\sigma_{0v'}/d\Omega(E_0, \theta)$ were accurately measured.

APPENDIX

Let $\sigma_{0j1j'}(E_0)$ be the cross section for the excitation process $(0, j) \rightarrow (1, j')$. In this article and the article[18] on elastic scattering we defined vibrationally elastic and inelastic cross sections as

$$\sigma_{0v'}(E_0) = \sum_{j'} \sigma_{00v'j'}(E_0) \qquad \text{(A. 1)}$$

with v' equal to 0 and 1 respectively. This treats the initial state as the ground state. But the measurements are made using a thermal distribution of rotational states. To test the effect of the distribution on the calculated results we replaced Eq. (A. 1) by

$$\sigma_{0v'}^{ave}(E_0) = 0.1748 \sum_{j'} \sigma_{00v'j'}(E_0) + 0.8252 \sum_{j'} \sigma_{02v'j'}(E_0) \,. \qquad \text{(A. 2)}$$

The coefficients are chosen to mimic the relative populations of the $(v=0,\ j=0)$ and $(v=0,\ j=2)$ states of N_2 at 300 °K. Similar averaging was performed for the differential cross sections. The results of the unaveraged [Eq. (A. 1)] and averaged [Eq. (A. 2)] treatments of the initial rotational state for an impact energy of 50 eV (with $0 \leq J \leq 20$ for both treatments) are given in Table VII. The table shows appreciable quantitative differences (up to about 30% for $d\sigma_{00}/d\Omega$ and over a factor of 2 for $d\sigma_{01}/d\Omega$) for different initial rotational states. But it is not clear which method is more suitable for comparing the present model to experiment. The results for initial state $(v=0,\ j=0)$ may be more accurate than those for $(v=0,\ j=2)$ because the omission of state $(v=0,\ j=4)$ in the expansion of the wavefunction may be a less serious approximation in the former case. Further a real thermal average would require more initial states with even larger values of j than 2. Thus we followed the simple unaveraged procedure here. But the reader should not forget this extra approximation in interpreting the comparison of theory and experiment.

*Supported in part by the National Science Foundation under grant numbers GP-28684 and MPS75-06416, by the National Aeronautics and Space Administration under contract number NAS7-100 to the Jet Propulsion Laboratory, by a research grant from the graduate school of the Unversity of Minnesota, and by a computing time subsidy from the University of Minnesota Computer Center.

†Alfred P. Sloan Research Fellow; Joint Institute for Laboratory Astrophysics Visiting Fellow, 1975–1976.

[1] R. S. Berry, Annu. Rev. Phys. Chem. 20, 357 (1969).
[2] S. Trajmar, J. K. Rice, and A. Kuppermann, Advan. Chem. Phys. 18, 15 (1970); S. Trajmar, J. K. Rice, A. Kuppermann, and D. G. Truhlar, Advan. Chem. Phys. 18, 70 (1970).
[3] E. N. Lassettre, Can. J. Chem. 47, 1733 (1969).
[4] S. Trajmar, D. G. Truhlar, J. K. Rice, and A. Kuppermann, J. Chem. Phys. 52, 4516 (1970).
[5] D. G. Truhlar and J. K. Rice, J. Chem. Phys. 52, 4480 (1970); erratum: 55, 2005 (1971).
[6] A. Skerbele, M. A. Dillon, and E. N. Lassettre, J. Chem. Phys. 49, 3543 (1968).
[7] A. Skerbele, M. A. Dillon, and E. N. Lassettre, J. Chem. Phys. 49, 5042 (1968).
[8] S. Trajmar, W. Williams, D. G. Truhlar, and D. C. Cartwright, Phys. Electron. At. Collisions Abstr. Paper. Int. Conf. 7, 1069 (1971).
[9] S. Trajmar, W. Williams, and A. Kuppermann, J. Chem. Phys. 56, 3759 (1972).
[10] Ž. Pavlović, M. J. W. Boness, A. Herzenberg, and G. J. Schulz, Phys. Rev. A 6, 676 (1972).
[11] D. G. Truhlar, S. Trajmar, and W. Williams, J. Chem. Phys. 57, 3250 (1972).
[12] D. G. Truhlar, J. Chem. Phys. 57, 3260 (1972).
[13] A. Chutjian, D. G. Truhlar, W. Williams, and S. Trajmar, Phys. Rev. Lett. 29, 1580 (1972).
[14] S. Trajmar, W. Williams, and A. Kuppermann, J. Chem. Phys. 58, 2521 (1973).
[15] Y. Itikawa, J. Phys. Soc. Jpn. 36, 1127 (1974).
[16] Reviews are given by G. J. Schulz, Rev. Mod. Phys. 45, 423 (1973); Ž. Pavlović, in *Physics of Ionized Gases: Proceedings of Invited Lectures given at the 7th Yugoslav Symposium and Summer School on the Physics of Ionized Gases*, Rovinj, Yugoslavia, 1974, edited by V. Vujnovic (Institute Jozef Stefan Ljubljana, Yugoslavia, 1974), p. 97; and G. J. Schulz, Dept. of Engineering and Applied Science, Yale University, Technical Report (29 April 1975).
[17] D. G. Truhlar, M. A. Brandt, A. Chutjian, S. K. Srivastava, and S. Trajmar, J. Chem. Phys. 65, 2962 (1976).
[18] M. A. Brandt, D. G. Truhlar, and F. A. Van-Catledge, J. Chem. Phys. 64, 4957 (1976).

[19]S. K. Srivastava, A. Chutjian, and S. Trajmar, J. Chem. Phys. **63**, 2659 (1975).
[20]A. Chutjian, J. Chem. Phys. **61**, 4279 (1974).
[21]S. K. Srivastava, A. Chutjian and S. Trajmar, J. Chem. Phys. **64**, 1340 (1976).
[22]J. W. McConkey and J. A.-Preston, J. Phys. B **8**, 63 (1975).
[23]D. G. Truhlar, F. A. Van-Catledge, and T. H. Dunning, Jr., J. Chem. Phys. **57**, 4788 (1972).
[24]P. G. Burke and N. Chandra, J. Phys. B **5**, 1696 (1972).
[25]D. G. Truhlar, J. K. Rice, S. Trajmar, and D. C. Cartwright, Chem. Phys. Lett. **9**, 299 (1971).
[26]S. Hara, J. Phys. Soc. Japan **22**, 710 (1967); M. E. Riley and D. G. Truhlar, J. Chem. Phys. **63**, 2182 (1975); R. Vanderpoorten, J. Phys. B **8**, 926 (1975); M. E. Riley and D. G. Truhlar, J. Chem. Phys. **65**, 792 (1976).
[27]See, e.g., D. Herrmann, K. Jost, J. Kessler, and M. Fink, J. Chem. Phys. **64**, 1 (1976).
[28]M. A. Crees and D. L. Moores, J. Phys. B **8**, L195 (1975).
[29]K. Takayanagi and S. Geltman, Phys. Rev. **138**, A1003 (1965).
[30]D. H. Sampson and M. C. Mjolsness, J. Chem. Phys. **57**, 3260 (1972).
[31]D. G. Truhlar (unpublished calculations).